

A Multifunctional Underwater Biomimetic Microrobot

Shuxiang Guo and Liwei Shi

Abstract Robots play an important role in underwater monitoring and recovery operations, such as pollution detection, submarine sampling and data collection, video mapping, and object recovery in dangerous places. However, regular-sized robots may not be suitable for applications in some restricted underwater environments. Accordingly, in previous research we designed several novel types of bio-inspired microrobots, using ionic polymer metal composite (IPMC) and shape memory alloy (SMA) actuators. These microrobots possess some of the attributes of compact structure, multifunctionality, flexibility, and precise positioning. However, they lack the attributes of long endurance, stable high speed, and large load capacity necessary for real-world applications. To overcome these disadvantages, we propose a mother–son robot system, composed of several microrobots as sons and a newly designed amphibious spherical robot as the mother. In this system, the mother robot is actuated by four water-jet propellers and eight servomotors, capable of providing stable high speed and carrying the microrobots to the desired target location where tasks are to be performed. Generally speaking, compact structure, multifunctionality, and precise positioning are considered incompatible characteristics for underwater microrobots. To realize the necessary multifunctionality for adapting to complex underwater environments, we introduce a walking biomimetic microrobot with two kinds of motion attitudes: a lying state and a standing state. The microrobot uses eleven IPMC actuators to move and two SMA actuators to change its motion attitude. In the lying state, the microrobot implements stick-insect-inspired walking/rotating motion, fishlike swimming motion, horizontal grasping motion, and floating motion. In the standing state, it implements inch-worm-inspired crawling motion in two horizontal directions and grasping motion in

S. Guo (✉) · L. Shi

School of Life Science, Beijing Institute of Technology, Beijing, China
e-mail: guo@eng.kagawa-u.ac.jp

L. Shi

e-mail: shiliwei@bit.edu.cn

S. Guo

Faculty of Engineering, Kagawa University, 2217-20 Hayashi-cho, Takamatsu,
Kagawa, Japan

the vertical direction. We constructed a prototype of this biomimetic microrobot and evaluated its walking, rotating, and floating speeds experimentally. The experimental results indicated that the robot could attain a maximum walking speed of 3.6 mm/s, a maximum rotational speed of 9 °/s, and a maximum floating speed of 7.14 mm/s. Obstacle-avoidance and swimming experiments were also carried out to demonstrate its multifunctionality.

Keywords Ionic polymer metal composite (IPMC) actuators · Biomimetic underwater microrobot · Motion attitudes · Micromechanism

1 Introduction

Robots are now widely used to implement underwater tasks considered by humans to be dangerous, dull, or dirty, primarily because of their long endurance, stable high speeds, and large load capabilities. This trend has continued into underwater monitoring and recovery operations, including pollution detection, submarine sampling and data collection, video mapping, exploration of unstructured underwater environments, object recovery in dangerous places, and other tasks [1, 2]. Various configurations, shapes, and sizes of underwater robots are required for different applications or tasks. For underwater environmental detection or observation, a compact structure with multifunctionality and flexibility enables a robot to work in limited spaces. When a large range of motions and large load capacity are required, a traditional motor-actuated electromagnetic structure is essential. When large interior space and flexible multidirectional rotation in a restricted space are required, a spherical robot body is recommended. When high-speed cruising is required, a streamlined robot body may be the best choice [3, 4].

If a robot is to be used in a complicated underwater environment, such as a narrow pipeline or a region filled with reefs, it should be endowed with the combined attributes of endurance, stable high speed, large load capability, flexibility, compact structure, and multifunctionality. Many types of underwater robots have been developed in recent years. While the use of some of these robots involves changing the angles of rudders or adjusting the differential propulsive forces of thrusters, a number of vectored propeller-actuated underwater robots have also been introduced [5]. A multi-channel Hall-effect thruster has also been reported, involving vector composition of Hall-effect thrusters [6]. Moreover, we have developed a spherical underwater robot equipped with three vectored water-jet-based thrusters [3]. However, most of these robots are steered by traditional electromagnetic thrusters, which are difficult to miniaturize [4].

Accordingly, motors are rarely found in microrobot applications [7, 8] and special actuator materials are used instead. A variety of smart materials, such as ionic polymer metal composite (IPMC), piezoelectric elements, pneumatic actuators, and shape memory alloy (SMA), have been investigated for use as artificial

muscles in new types of microrobots [9–15]. In this research, IPMC is used as actuator material to develop a microrobot with a compact structure, multifunctionality, and flexibility. The actuation characteristics of IPMC, which include suitable response time, high bending deformation and long life, show a significant potential for the propulsion of underwater microrobots [16–21]. Although many biomimetic microrobots with smart actuators have been introduced in recent years, developing a single microrobot with compact structure, flexibility, and multifunctions remains a challenge, due to conflicts between the three characteristics [4]. For this reason, many microrobot designers have abandoned compact structure in favor of biomimetic multi-jointed configurations to improve flexibility and obtain multifunctions. Others have sacrificed flexibility and multifunctions in pursuit of miniaturization.

For real-world applications, an underwater robot should possess the attributes of endurance, stable high speed, large load capacity, flexibility, compact structure, and multifunctionality. To implement these characteristics, we propose a mother–son robot system, which includes several microrobots as sons and a newly designed amphibious spherical robot as the mother. This is an original concept and is inspired by the design of aircraft carrier systems [4]. In this system, the mother robot is actuated by four water-jet propellers and eight servomotors, capable of providing stable high speed and carrying the microrobots to the desired target location where tasks are to be performed. When the mother robot reaches the desired location, or encounters a narrow channel that is difficult to navigate, it assumes a stable position and acts as a base station for the microrobots. Then, the microrobots exit the mother robot, proceed to the target position, and carry out their tasks.

Compared with a single large robot, when the final tasks are carried out by microrobots, it is easier to adapt to narrow environments and implement relatively high positioning precision. In addition, compared with individual microrobots, the mother–son system offers the following advantages.

- (1) The range of motions of the overall system is expanded, owing to the relatively high speed and endurance of the mother robot.
- (2) The microrobots can obtain a relatively stable, high power supply via cables.
- (3) Since the microrobots are all controlled by the mother robot, communications between microrobots can be implemented by the mother when cooperation is needed.
- (4) Since the power supply and control units are installed in the mother robot, the microrobots can be designed with a more compact structure, suitable for restricted spaces such as narrow pipelines or channels.

We introduced a newly designed spherical amphibious mother robot in [22–24]. A spherical body has both a compact structure and maximum interior space, compared to a streamlined body. It can rotate and change direction more easily than a streamlined design, which is very important for microrobots in restricted spaces. Following the mother robot in previous researches, this chapter will mainly focus on the microrobots. At the end of this chapter, we will show a schematic diagram to illustrate the mother-son system.

Aside from fishlike and manta-ray-like swimming locomotion, we have developed several microrobots that employ biomimetic locomotion to implement walking, floating and swimming motions [1, 2, 25–27]. However, each of these units implements only some of these motions and none of them are able to carry out simple tasks such as grasping and carrying objects to a desired position, detecting an object, or avoiding an obstacle. To realize the necessary multifunctionality for adapting to different environments, a hybrid underwater microrobot with two motion attitudes is introduced in this paper. The microrobot uses eleven IPMC actuators to implement three-dimensional underwater motions, and two SMA actuators for attitude change. The robot can change between two attitudes: a lying attitude and a standing attitude. It uses the standing attitude to cross a high, narrow gap, and changes to the lying attitude while walking through a low, wide tunnel. We have constructed a prototype microrobot and carried out a series of experiments to evaluate its performance.

The remainder of this chapter is divided into four parts. First, we describe the characteristics of IPMC actuators and summarize the implemented techniques of underwater locomotion. Second, we review the feasibility results for several previously developed microrobots. Third, based on several types of biomimetic locomotion, we introduce the new hybrid microrobot design, including the structural design and motion mechanisms in the two attitudes. Fourth, we discuss the construction of a prototype of this hybrid microrobot, together with a series of experiments to evaluate its walking, rotating, floating, and swimming speeds. Attitude change and obstacle-avoidance experiments are also included. Finally, we present our conclusions.

2 Biomimetic Locomotion

2.1 IPMC Actuators

(1) IPMC is an innovative material made of an ionic polymer membrane, chemically plated with gold electrodes on both sides. When an electrical stimulus is applied across the thickness of the IPMC, bending deformation will be generated for the water molecules' redistribution in the ionic polymer membrane, which expands the cathode side of the membrane and contract the anode side. Its actuation characteristics show significant potential for the propulsion of underwater microrobots. It is lightweight and has a suitable response time, high bending deformation, and long life. IPMC is widely used in soft robotic actuators such as artificial muscles, as well as on dynamic sensors [16]. The IPMC adopted for this research consists of Au deposited on NafionTM film with a thickness of 0.22 mm.

An IPMC actuator can be regarded as equivalent to a cantilever beam. Figure 1 shows the mechanical configuration and relevant geometrical parameters, which are as follows: L_c denotes the length of the clamped part of the IPMC, L_f is the total free

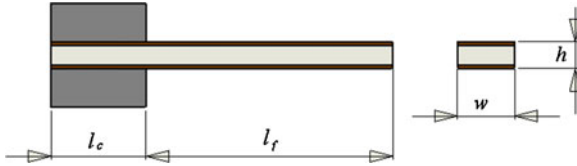


Fig. 1 Mechanical configuration of the actuator and relevant parameters

length of the IPMC, and w and h denote the width and the height of the IPMC cross-section. The pinned end is used to apply electrical voltages across the thickness.

According to mechanical analysis, bending deformation of an IPMC actuator results from the redistribution of internal water molecules. Under the influence of an applied stimulus, the water molecules in the actuator are redistributed in the following two stages [28].

(2) When an electrical stimulus is applied across the thickness of the IPMC, each hydrated sodium ion moves to the cathode side, accompanied by four hydrated water molecules. Bending deformation is then generated by the expansion of Nafion117 near the cathode side and contraction near the anode side.

(3) After a short time, the self-diffusion of water molecules causes free water molecules to gradually flow to the anode side, reducing the concentration of water molecules at the cathode and demonstrating the deformation recovery potential of the IPMC actuator.

We measured the free-end deflection of an IPMC actuator in a water tank for different applied square-wave signals. The sample IPMC actuator was 20 mm long, 4 mm wide, and 0.22 mm thick. It was driven by a personal computer (PC) equipped with a digital-to-analog converter card, and the deflection of the IPMC was measured via a laser displacement sensor. The laser sensor was used to translate the displacement to a voltage and then the voltages were recorded and translated to the PC by an analog-to-digital converter card. We used the square-wave signals to drive the IPMC actuator. Figure 2 indicates that the displacement was inversely proportional to the frequency of the input signal, and proportional to the input voltage at a low frequency. However, the displacement variation with respect to voltage was greatly reduced at a high frequency [29].

We also measured the bending force generated at the free end of the equivalent cantilever beam by applying different signals. In this experiment, the sample IPMC actuator was 24 mm long, 18 mm wide, and 0.22 mm thick. The actuator was driven by a PC equipped with a digital-to-analog converter card, and the bending force of the IPMC was measured by an electronic balance. To reduce the torque on the electronic balance, we used a needle to transfer the press force from the IPMC actuator. The initial distance between the IPMC and the needle tip is set as 3 mm. Figure 3 shows the experimentally recorded tip-bending force of the actuator for different voltages. The experimental results indicate that the tip-bending force increases as the driving voltage increases [30].

Fig. 2 Tip displacements of the IPMC actuator [29]

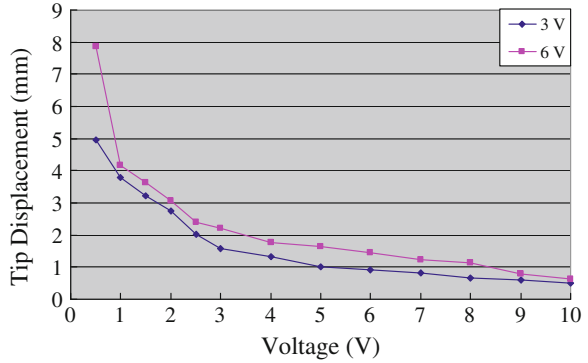
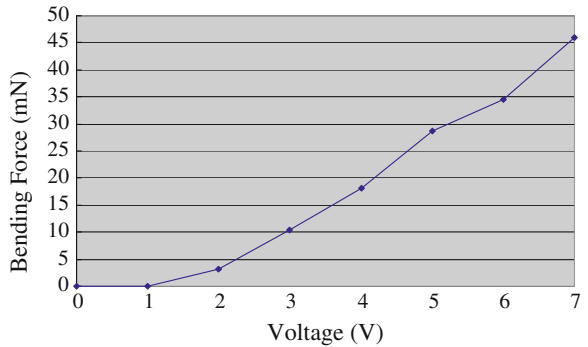


Fig. 3 Bending forces of the IPMC actuator [30]



2.2 Bio-inspired Locomotion

IPMC actuators can be used as oscillating or undulating fins for swimming microrobots when a fast response is required [16–18, 31, 32]. However, this type of swimming motion cannot ensure precise positioning of the robot. Furthermore, fishlike propulsion mechanisms simply mimic the undulating and oscillatory body/fin motions of a fish. Some simple underwater tasks are not easily carried out without hands or fingers. Therefore, in addition to swimming, other types of biomimetic locomotion are required for microrobots with compact structure, multi-functions, and flexibility.

2.2.1 Stick Insect-Inspired Walking Locomotion

Nature provides perfect models for robots. Biomimetic robots borrow their senses and structure from animals, such as insects, fish, and birds. In the case of the stick insect, each leg is composed of the coxa, femur, tibiae, and tarsus. The tarsus is also

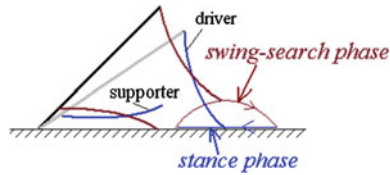


Fig. 4 Two-phase driving locomotion with IPMC actuators [25]

called the foot and does not contribute to its movements. The coxa offers the foot one degree of freedom (DOF) in the direction of movement. The femur and the tibiae offer the foot two DOF to enable it to find a reliable foothold during the swing–search phase to touch the ground and support the body during the stance phase.

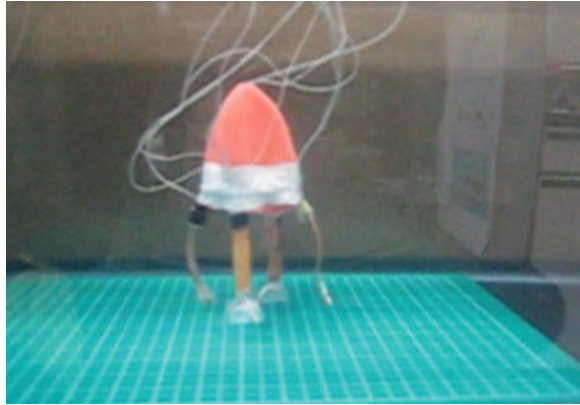
A stick insect-inspired biomimetic locomotion prototype using two IPMC actuators was introduced in [1]. As Fig. 4 shows, the actuator in the vertical direction is called the driver, while the actuator in the horizontal direction is called the supporter. The free end of the driver is the foot. Each step cycle can be separated into four periods. First, the supporter lifts the body up, and the driver is off the ground. Second, the driver bends forward. Third, the supporter bends upward far enough so that it is off the ground, while the driver in contact with the ground supports the body. Fourth, the driver bends backward in the propulsion stroke, and the body is pushed forward. The driver and supporter are controlled by two channels of square waves, each with the same frequency. The phase of the supporter lags 90° behind that of the driver [1, 2, 25].

2.2.2 Jellyfish-like Floating Locomotion

Jellyfish movement is dependent on floatation, ocean currents, and winds and is accomplished via a form of jet propulsion. Specifically, jellyfish move by squeezing their bodies so that jets of water are ejected from underneath, propelling them forward.

A jellyfish-inspired biomimetic locomotion prototype with SMA actuators was introduced in [1, 33]. The jellyfish-inspired body uses SMA actuators to imitate the circular muscles of a real jellyfish, as shown in Fig. 5. The body shrinks when voltage is applied and water is squeezed out of it. This changes the buoyancy and produces an upward force. The body floats upward when the force reaches a certain value. The upward force can be changed by controlling the frequency of the actuator shrinkage and the voltage between its two ends. This means that the microrobot can be induced to float upward, remain neutrally buoyant, or sink as required.

Fig. 5 A jellyfish-inspired biomimetic locomotion prototype [1]



2.2.3 Butterfly-Inspired Swimming Locomotion

Butterfly movement is accomplished by the counter force of air. Specifically, they flap their wings to push the air at different frequencies and speeds. In a single flapping period, there are two motions, folding and unfolding. Movement results from the fact that the folding motion pushes the air between their wings at a higher speed than the unfolding motion.

A butterfly-inspired biomimetic locomotion prototype with SMA actuator was also introduced to implement fast swimming. We use two pectoral fins to imitate the flapping motions of a butterfly. The fins are installed perpendicular to the horizontal plane, and the initial angle between them is set at $\pi/3$. They squeeze the water between them to create a counter force in the horizontal direction. In this way, the microrobot can be induced to implement a swimming motion. The horizontal propulsion can be changed by controlling the frequency of the actuator shrinkage and the driving voltage. The two pectoral fins are driven by separate SMA actuators, and thus the robot can swim or make turns via the cooperation of the fins, as shown in Fig. 6 [27].

2.2.4 Inchworm-Inspired Crawling Locomotion

Inchworms have smooth, hairless bodies, usually about 25 mm long. Also known as measuring worms, spanworms, or loopers, they lack appendages in their midsections, causing them to have a characteristic looping gait. They have three pairs of true legs at the front end, like other caterpillars, but only two or three pairs of prolegs at the rear end. An inchworm moves by drawing its hind end forward while holding on with its front legs, and then advancing its front section while holding on with its prolegs [26, 34, 35].

An inchworm-inspired biomimetic locomotion prototype with two IPMC actuators was introduced to implement fast creeping. The design was based on a one

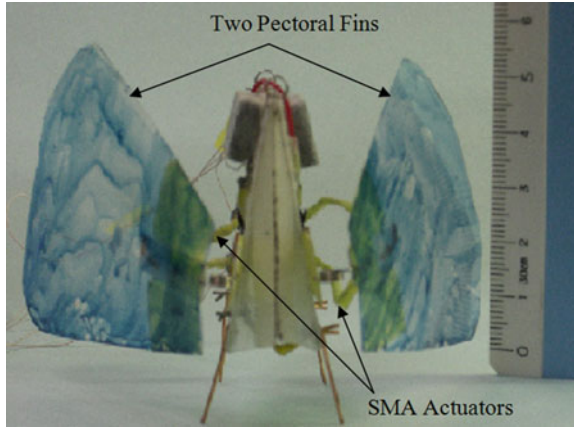


Fig. 6 A butterfly-inspired biomimetic locomotion prototype [27]



Fig. 7 An inchworm-inspired biomimetic locomotion [35]

DOF leg. The structure of the one DOF walking mechanism is described in [35]. This mechanism can only implement crawling motion, as shown in Fig. 7.

3 Developed Microrobots

Swimming motion is a universal motion in water for the underwater species. Till date, the majority of research work has been focused on fish-like propulsion mechanisms, fin materials, remote operation, multi-agent cooperation, and

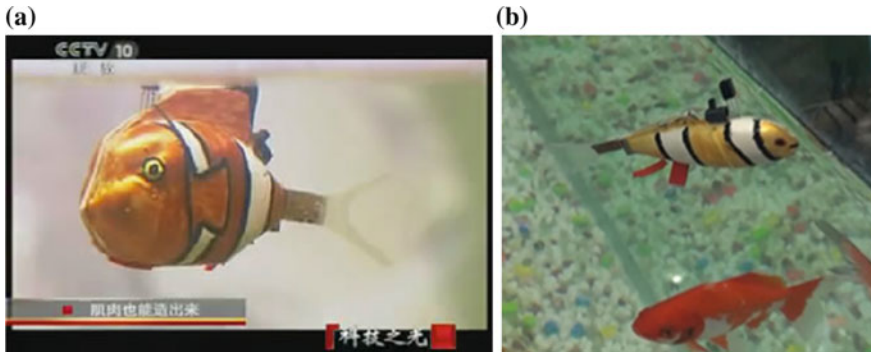


Fig. 8 Fish-inspired microrobot [32, 36]. **a** Fish-like microrobot. **b** Living with the real fish

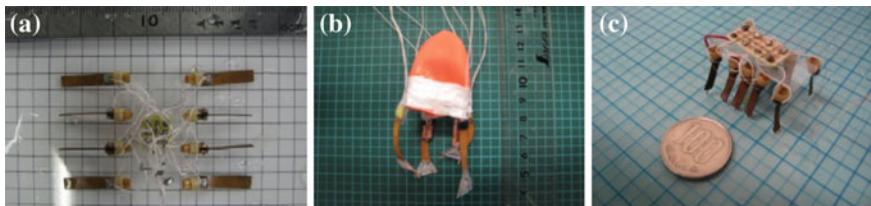


Fig. 9 Prototype microrobots. **a** Stick insect-inspired [2]. **b** Jellyfish-inspired [1]. **c** Inchworm-inspired [26, 35]

mechanical structures. We have developed a robotic fish by using one IPMC actuator, which was reported by CCTV 10 in China. Figure 8 shows this fishlike microrobot, which can live with real fish in the same water tank.

However, the swimming motion cannot ensure the position precision for the robot. Also, the fishlike propulsion mechanisms just mimic the undulating and oscillatory body/fin motions. It is hard to implement some simple underwater tasks without hands or fingers. So, besides the swimming, we proposed some other biomimetic locomotion.

Based on stick insect-inspired walking locomotion, a prototype of an eight-legged microrobot was developed, as shown in Fig. 9a [2]. It was 33 mm long, 56 mm wide, and 9 mm high. Four legs were used as drivers and the other four actuators were used as supporters. It was capable of walking, rotating, and diving/surfacing. However, the floating efficiency of this microrobot was not high. To improve the floating motion, a prototype of a jellyfish-type microrobot was constructed, based on jellyfish-inspired locomotion, as shown in Fig. 9b [1]. It was 68 mm high, with a weight of 4.81 g in air. This biomimetic microrobot consisted of a two-ring body and four legs. The body was designed to imitate a jellyfish's diving/surfacing motions. Additionally, four IPMC actuators were fixed on the body to implement walking motion in two directions. Although the floating motion

was improved, the prototype was unable to rotate, and the walking motion was unsatisfactory because the center of gravity was located in one of the two halves of the body, causing an imbalance in the overall body and a large amount of slippage.

For the purpose of creating a microrobot with a compact structure and multi-functions, an inchworm-inspired microrobot with ten IPMC actuators was developed, as shown in Fig. 9c. It was 33 mm long, 14 mm wide, and 14 mm high. Four outside actuators were used as legs to implement walking, rotating, and floating motions. The other six actuators were used as fingers to grasp small objects [26, 34, 35]. Figure 10 shows the hybrid motion of the inchworm-inspired microrobot. Compared with the jellyfish-like robot, this design offered the advantages of stability, compact structure, less water resistance, and grasping motion implementation. However, because the rotating radii were not the same for the outside four legs, a large amount of slippage

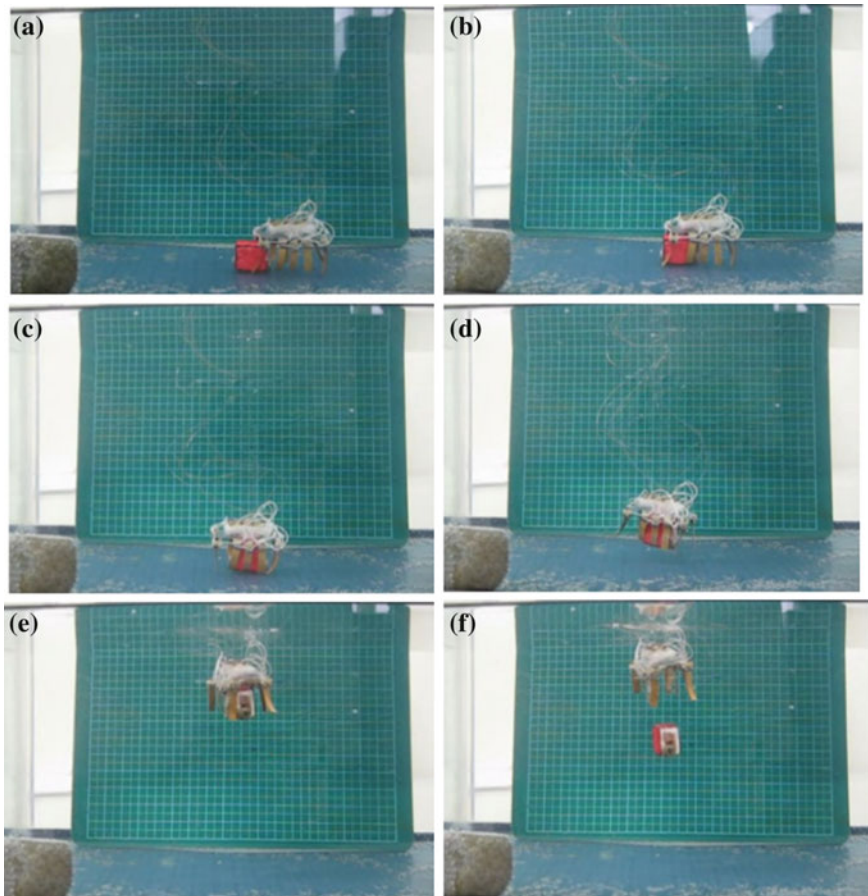
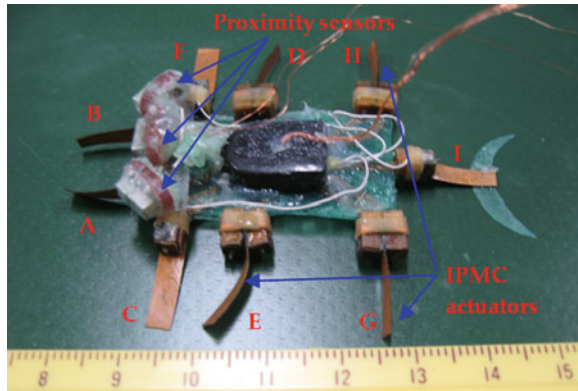


Fig. 10 Hybrid motion of the inchworm-inspired microrobot. **a** Initial position. **b** Walking motion. **c** Grasping motion. **d** Floating motion. **e** Reaching the surface. **f** Opening motion

Fig. 11 Prototype lobster-like microrobot



occurred while rotating and the rotating efficiency was not high. Only the outside four legs were used to electrolyze the water around the IPMC surface, generating air bubbles, which became attached to the surfaces of the legs, increasing the buoyancy and implementing the floating motion. Due to the limitations of the structure, the inside six legs were used solely as fingers to grasp an object and could not contribute any buoyancy to the floating motion, so that the floating speed was slow. To inherit the multifunctions of the inchworm-inspired microrobot and overcome its disadvantages, we introduced a new lobster-like microrobot, intended for underwater exploration in a restricted space, as shown in Fig. 11. It uses nine IPMC actuators as legs or claws. Seven actuators are used as legs to implement walking, rotating, and floating. The other two actuators are used as claws to grasp small objects. To imitate the antennae of actual lobsters, three infrared proximity sensors are installed on the head of the microrobot to detect an obstacle. To realize the necessary multifunctionality for adapting to different environments, a hybrid underwater microrobot with two motion attitudes will be introduced in the following sections.

4 Proposed Multifunctional Microrobot

4.1 Structure of the Microrobot

Based on the above types of biomimetic locomotion, we propose a hybrid underwater microrobot, consisting of a plastic body, eleven IPMC actuators, two SMA actuators, a passive tail fin, and two plastic sheets. With the SMA actuators affixed to the plastic sheets, the microrobot can change its attitude between the lying state and the standing state, as illustrated in Fig. 12. The body of the microrobot is 35 mm long and 20 mm wide, as determined by the motion functions and balance of the overall body. It is 3 mm high in the lying state and 21 mm high in the standing state. The eleven actuators are all 17 mm long, 3 mm wide, and 0.2 mm thick.

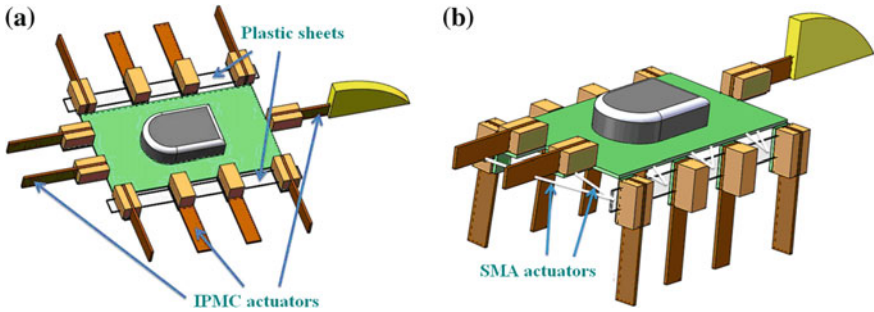
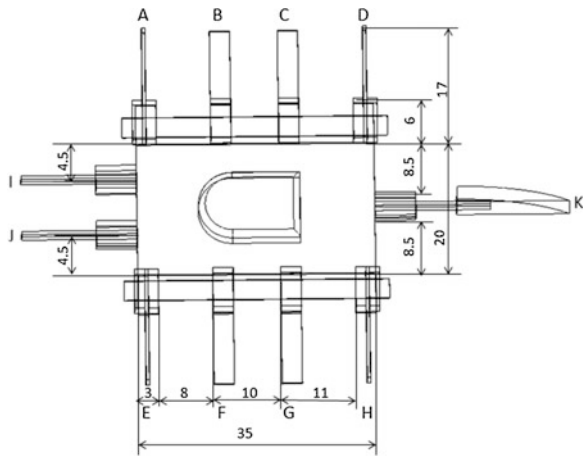


Fig. 12 Proposed hybrid microrobot. **a** Lying attitude. **b** Standing attitude

Fig. 13 Leg sequence and dimensions of the proposed microrobot



The microrobot uses eleven 1-DOF IPMC actuators to realize walking, rotating, grasping, swimming, and floating motions [37]. Figure 13 shows the leg sequence of these actuators. In the lying attitude, actuators I and J are used as fingers, and are designed for grasping. Actuators B, C, F, and G are called supporters, while actuators A, D, E, and H are called drivers. By changing the bending directions of the four drivers, the robot can walk forward or backward, and rotate clockwise or counterclockwise. In the standing attitude, actuators B, C, F, and G are used as fingers for grasping. Legs A and E are used as leading legs, while legs D and H are used as following legs to implement walking and rotating motions. In both attitudes, actuator K is used to actuate the passive tail fin for swimming.

4.2 Force Analysis of the Attitude Change

The SMA actuators are used to change the attitude of the proposed microrobot. It was necessary to calculate the force required for standing motion before attaching the SMA actuators to the robot body. We then constructed a physical mechanism to transform horizontal forces into vertical forces that could be measured with a spring dynamometer. Figure 14 shows a diagram of the force transition mechanism. We first inserted two fishing lines through the points A–D and B–C, respectively, and then connected the four ends of the two lines at the point O. The vertical force F was measured via a spring dynamometer at point O. The force F_n required to pull the plastic sheet from the horizontal to the vertical direction is given by

$$F_n = 2F_3 \tag{1}$$

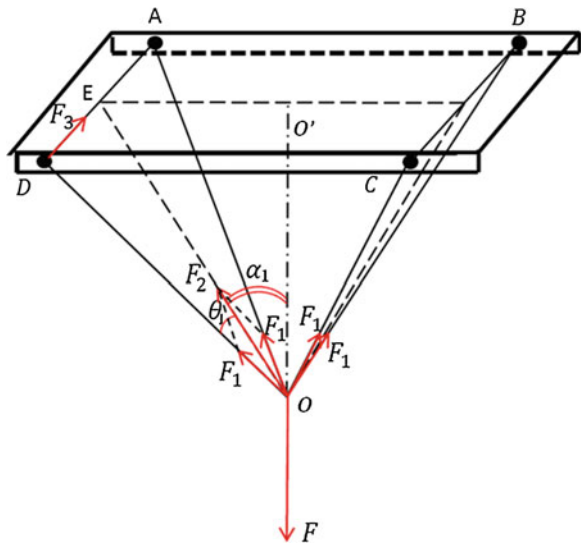
where F_3 denotes the tensile force in either of the lines (AD or BC). According to Fig. 14, the tensile forces F_3 and F_1 and the resultant force F_2 can be obtained from the following equations:

$$F_3 = -F_1 \sin \theta_1 \tag{2}$$

$$F_1 = \frac{F_2}{2 \cos \theta_1} \tag{3}$$

$$F_2 = -\frac{F}{2 \cos \alpha_1} \tag{4}$$

Fig. 14 The scheme of tensile force measurement for the attitude change



where F denotes the measured vertical force.

Utilizing (1)–(4), F_n is given by

$$F_n = \frac{F \sin \theta_1}{2 \cos \theta_1 \cos \alpha_1} \quad (5)$$

We used this formula to calculate the force F_n required for our proposed structure.

4.3 Mechanism of the Walking/Rotating Motion in the Lying Attitude

In the lying attitude, the proposed microrobot can implement stick-insect-inspired walking motions using supporters B, C, F, and G and drivers A, D, E, and H. The drivers provide the propulsion for the motion, and the supporters are employed to raise the drivers off the ground and reduce the resistance. The drivers and supporters are controlled by two square-wave channels, each with the same frequency. The phase of the four supporters lags 90° behind that of drivers. Figure 15 shows a single step cycle of the forward motion. Each cycle is divided into four periods as follows [1].

- (1) The four supporters lift the body to raise the drivers off the ground.
- (2) As the supporters lift the body, the drivers bend forward.
- (3) The four supporters bend upward, causing the four drivers to contact the ground.
- (4) The four drivers bend backward to push the body forward.

The walking speed is determined by the displacements of the four drivers and the frequency of the control signal. Since the drivers are distributed symmetrically on both sides of the body, and have the same size and deflection characteristics, they bear equivalent loads and drag forces. Therefore, all four drivers provide the same tip displacement for a given applied input voltage. Assuming that the robot is moved by a fixed driving voltage and current, the tip displacement of the actuator in one direction is $d/2$, and the distance the robot advances is d , as shown in Fig. 15c, d. The walking speed can then be obtained from

$$v = d \times f = (d_0 - \Delta d) \times f \quad (6)$$

where v denotes the average walking speed, d_0 denotes the tip displacement of a driver without a payload, Δd is the reduction in the actual displacement of a driver due to friction, and f is the frequency of the input signal.

By changing the bending directions of the four drivers, forward and backward walking motions and clockwise and counterclockwise rotations can be implemented. Figure 16 shows a single step cycle of the rotational motion, which can also be divided into four periods. When the four supporters lift the body, the two left drivers bend backward and the two right drivers bend forward. When the four

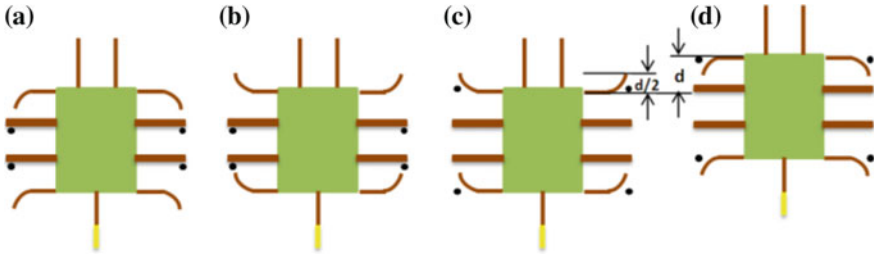


Fig. 15 One step cycle of moving forward motion in lying structure (The marks • indicate which actuator contacts the ground). **a** The supporters lift the body. **b** The drivers bend forward. **c** The supporters bend upward. **d** The drivers bend backward

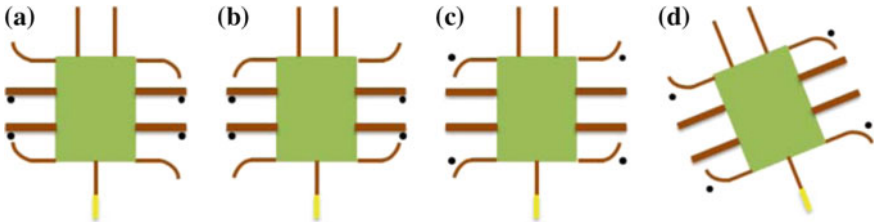


Fig. 16 One step cycle of rotating motion in lying structure (The marks • indicate which actuator contacts the ground). **a** The supporters lift the body. **b** The two left drivers bend backward and the two right drivers bend forward. **c** The supporters bend upward. **d** The two left drivers bend forward and the two right drivers bend backward

supporters bend upward, the four drivers contact the ground and bend in the reverse direction.

When the rotational direction of drivers E and H is opposite to that of drivers A and D, the microrobot can implement clockwise rotation or counterclockwise rotation. The robot rotates through the angle θ in a single step cycle, as shown in Fig. 17a. Here, θ is given by

$$\theta = \frac{L}{R} \tag{7}$$

where L denotes the length of the rotational arc and R denotes the radius of rotation with center-point O . From Fig. 17b, we have

$$r \cos \alpha = r - \frac{d}{2} \tag{8}$$

$$l = \alpha \times r \tag{9}$$

$$h = \sqrt{\frac{d}{2} \cdot \left| 2r - \frac{d}{2} \right|} \tag{10}$$

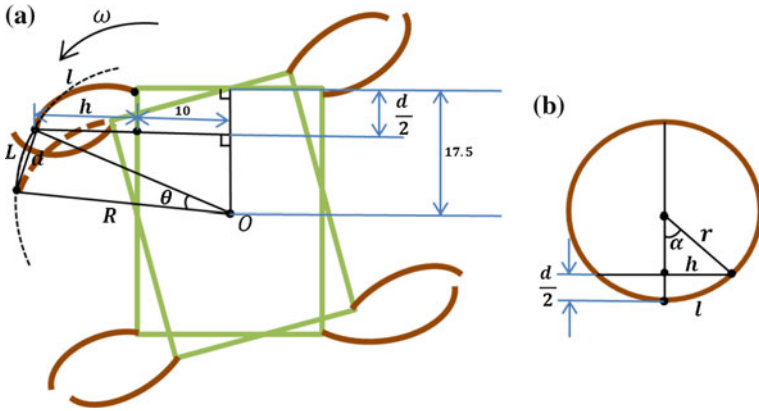


Fig. 17 **a** The rotating angle in one step cycle. **b** The calculation of the value of h (only drivers are drawn)

where r is the bending radius of the IPMC actuator, α denotes the central angle of the IPMC bending arc, l denotes the length of the IPMC actuator, and h denotes the semifocal chord length of the IPMC bending arc. The radius R can be calculated using the equation

$$R = \sqrt{(h + 10)^2 + (17.5 - \frac{d}{2})^2} \tag{11}$$

When d is very small, we can approximate the arc length L by d , the linear distance between the initial and final robot position. According to Eqs. (7) and (11), the theoretical rotational speed can then be calculated from

$$\omega = \theta * f = \frac{2d}{\sqrt{(h + 10)^2 + (17.5 - \frac{d}{2})^2}} f \tag{12}$$

4.4 Mechanism of the Walking/Rotating Motion in the Standing Attitude

In the standing attitude, the microrobot can implement inchworm-inspired crawling motions in two directions (longitudinal and transverse) using the eight legs A–H. Unlike the motions in the lying attitude, legs A and E are used as leading legs, while legs D and H are used as following legs. This allows the robot to implement walking motion in the longitudinal direction. When the robot walks forward, the phase of the leading leg lags 90° behind that of the following leg, as shown in Fig. 18 [35]. In this attitude, the robot can fold all legs below its body to get across

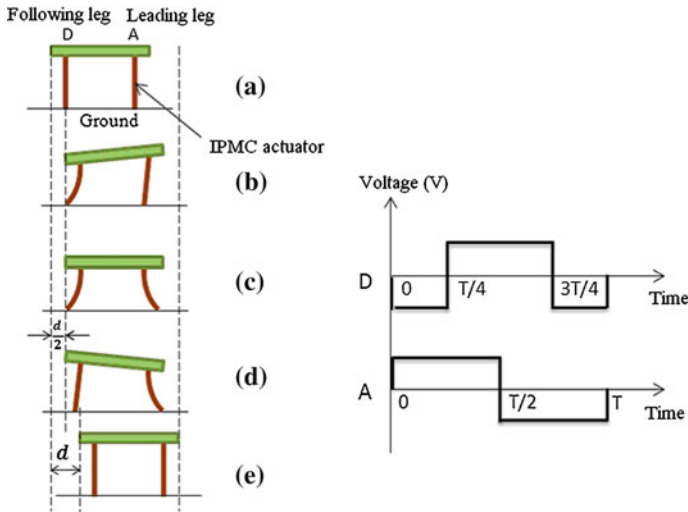


Fig. 18 One step cycle of crawling motion in standing attitude [35]

high narrow gaps. The crawling speed in the standing attitude is determined by the same parameters as in the lying attitude.

Based on this walking mechanism, when one side of the microrobot moves forward and the other side moves backward, or remains stationary, the robot can rotate in either the clockwise or counterclockwise direction. The rotational speed of the robot is determined by the rotational angle in a single step and the frequency [35].

4.5 Mechanism of the Grasping Motion

In the lying attitude, the microrobot can grasp small objects and carry them to a specified location using fingers I and J. First, the microrobot moves close to the object using legs A–H. Second, fingers I and J bend toward each other to grasp the object. Then the microrobot carries the object to the desired destination. In the standing attitude, the microrobot can also grasp small objects using the leg pairs B–F and C–G for this purpose, while legs A, D, E, and H provide the crawling and rotational motions.

4.6 Mechanism of the Floating Motion

When the frequency of the driving voltage is decreased to 0.3 Hz, the water around the IPMC actuators is electrolyzed. Air bubbles are generated and become attached

to the leg surfaces, and the buoyancy of the microrobot is increased. In the lying attitude, four drivers and four supporters are used to electrolyze the water and implement floating motion. In the standing attitude, leg pairs A–E and D–H are used to implement floating motion. The tail fin can also be used to provide buoyancy, and to adjust the balance of the overall body while floating.

4.7 Mechanism of the Swimming Motion

In a similar manner to the BCF and MPF locomotion of fish, robots can be classified into body and/or caudal actuator (BCA) types, and median and/or paired actuator (MPA) types [38]. The proposed microrobot utilizes the BCA mode, which generates thrust by bending the caudal fin K, as shown in Fig. 13. The bending of the caudal fin provides oscillatory motion, and is triggered by a single IPMC actuator. A passive fin is attached to the free end of this actuator to increase the thrust.

5 Prototype Microrobot and Experiments

5.1 Prototype Microrobot

Based on the proposed structure, a prototype hybrid underwater microrobot with two motion attitudes was constructed, as shown in Fig. 19. The body was composed of two layers, to which eleven IPMC actuators were attached with wooden clips. Two IPMC fingers and a tail fin were attached to the first layer, while eight IPMC legs were attached to the second layer. Two SMA actuators were affixed to two sheets attached to the second layer. The prototype microrobot employed eight legs to walk, rotate, and float in two attitudes. Two fingers were utilized to implement grasping, and the tail fin was used for swimming. The control signals of the IPMC actuators were all square waves, in order to drive the actuators more efficiently [29].

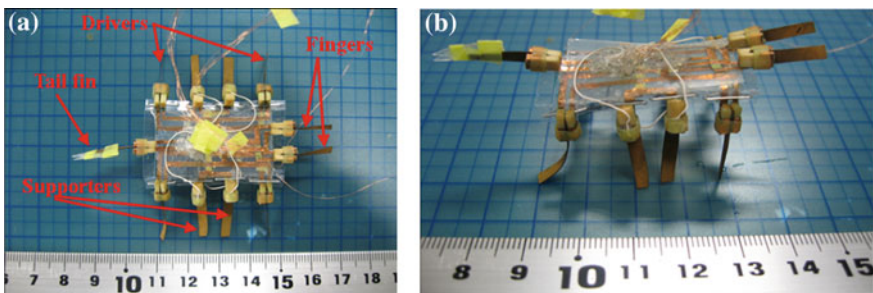


Fig. 19 The prototype microrobot (in air). a The lying attitude. b The standing attitude

In addition, two SMA actuators were employed to pull the two sheets and fold the eight legs below the body, to implement the attitude change. The prototype driving system consisted of an AVR atmega16 and twelve Omron G6 K-2P electric relays that were used as circuit changers to vary the input voltages. The microrobot received its control signals through enamel-covered wires with a diameter of 0.03 mm. The wires were soft enough for their resistance to be ignored [29].

5.2 Walking, Rotating, and Grasping Experiments in the Lying Attitude on an Underwater Flat

The walking experiments were conducted on a flat underwater surface. In these experiments, we varied the applied signals, and calculated the walking speed by recording the time required to cover a distance of 50 mm. The experiment was repeated five times for each set of control signals to obtain an average speed.

At a fixed current of 0.7 A, we carried out two groups of experiments with different applied voltages and frequencies. Figure 20 shows the experimental results for voltages of 4 and 6 V, which indicated that the walking speed was proportional to the input voltage, and that the walking motion was highly efficient in the control frequency range from 2 to 6 Hz. We can see that: (1) the walking speed increased with the input voltage; (2) at 6 V, a maximum speed of 3.6 mm/s was attained at 2.5 Hz; and (3) at 4 V, a maximum speed of 2.1 mm/s was attained at 2.5 Hz. When the frequency was higher than 7 Hz, the walking speed approached 0.

At a fixed frequency of 1 Hz, we also carried out three groups of experiments with applied voltages 3, 5 and 8 V. We obtained an average speed for every set of signals, varying the current as shown in Fig. 21. From the results, the walking speed was proportional to the applied current and input voltage. The microrobot required only low current and voltage for walking motion in the lying attitude.

Fig. 20 Experimental walking speeds with different frequencies

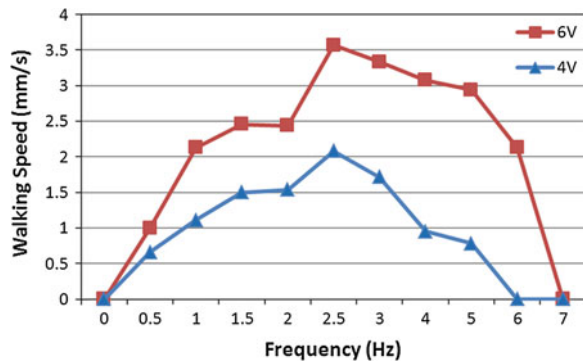


Fig. 21 Experimental walking speeds with different currents

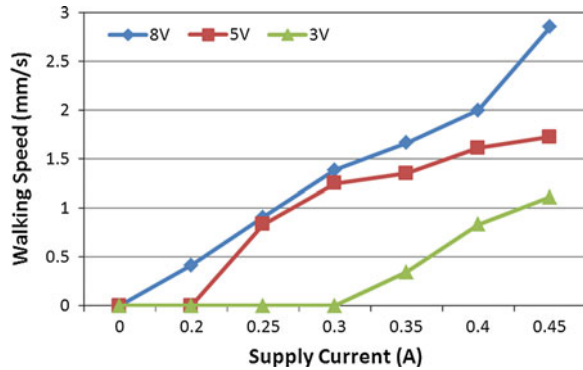
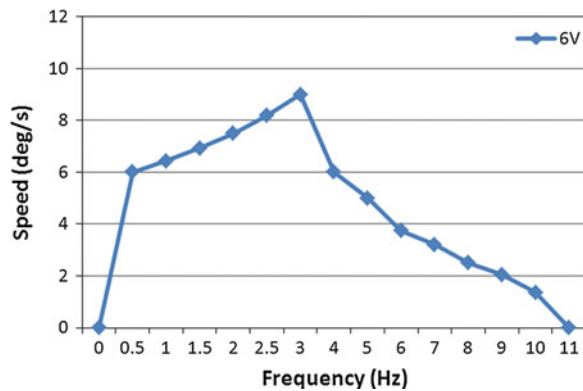


Fig. 22 Experimental rotating speeds



In the rotating experiments, we varied the control frequency from 0.5 to 11 Hz at a fixed voltage of 6 V and a fixed current of 1 A, and calculated the average rotational speeds. Figure 22 shows the experimental results, which indicated that the microrobot had a higher rotational speed in the frequency range from 0.5 to 4 Hz, and a maximum rotational speed of 9 °/s. When the control frequency was lower than 3 Hz, the rotational speed was proportional to the frequency, since the oscillatory amplitude was relatively large. However, when the control frequency was higher than 3 Hz, the rotational speed was inversely proportional to the frequency, since the rotational angle in a single step cycle became small, and the decreased displacement became a primary factor affecting the rotational speed.

In the lying attitude, the microrobot was able to use its two fingers to implement grasping motion. A hybrid walking, rotating, and grasping motion is shown in Fig. 23. First, the robot walked forward. Second, it rotated clockwise and opened its two fingers. Then it closed its fingers and rotated counterclockwise. Finally, it walked backward.

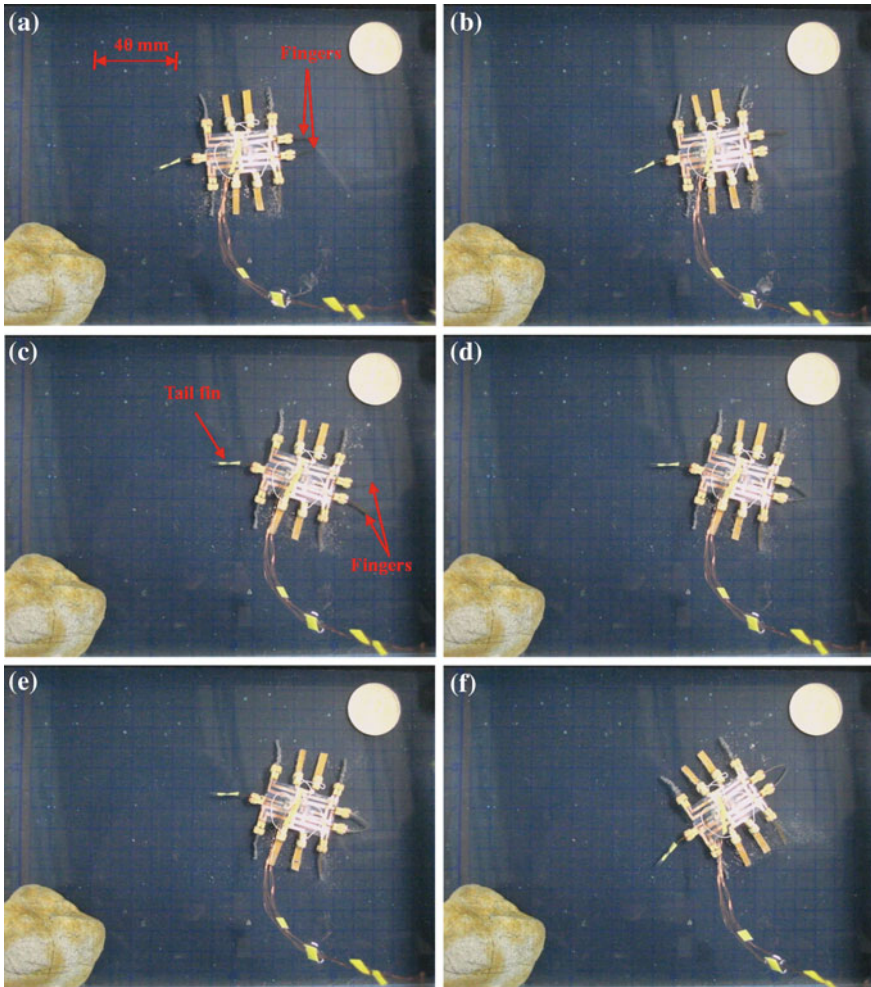


Fig. 23 Walking, rotating, and grasping motions. **a** Walking forward. **b** *Right* turning. **c** Two fingers open. **d** Grasping motion. **e** *Left* turning. **f** Walking backward

5.3 Floating Experiments Without Payloads

Legs A–H were used to electrolyze the water and implement floating motion. In the floating experiments, we varied the frequencies of the driving voltages and calculated the floating speed by recording the time required to float through a vertical distance of 100 mm. Figure 24 shows a video sequence of the floating motion.

At a fixed voltage of 6 V, we varied the control frequencies from 0.05 to 0.5 Hz. The experiment was repeated 5 times for each set of control signals to obtain an average speed. Figure 25 shows the experimental floating speeds for different

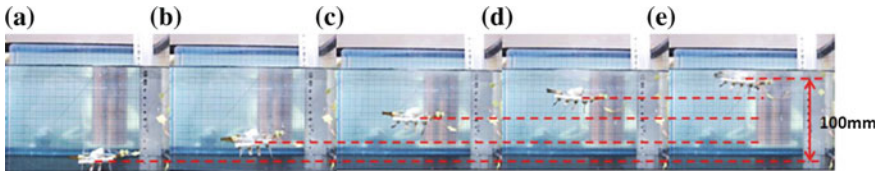
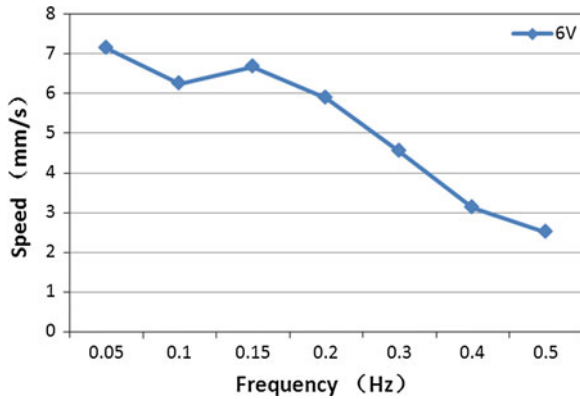


Fig. 24 Floating experiment. a Phase 1. b Phase 2. c Phase 3. d Phase 4. e Phase 5

Fig. 25 Experimental floating speeds



frequencies. From the results, the average floating speed was inversely proportional to the control frequency, and the maximum speed was achieved with a frequency of 0.05 Hz.

5.4 Standing Experiments

In the standing experiments, we used the two SMA actuators to make the microrobot stand up, both in air and on the underwater flat. Figure 26 shows video sequences of the standing motion on the underwater flat, from the front and left-side perspectives. We carried out the experiments with a control voltage of 8 V and a maximum current of 1 A. An initially deformed SMA actuator can recover its predetermined low-temperature shape during heating, demonstrating the shape memory effect [39]. Therefore, thermal insulation is important for SMA actuators, especially in water. Accordingly, we sealed the two SMA actuators with elastic adhesive tape to achieve a better heating effect when they were triggered to shrink.

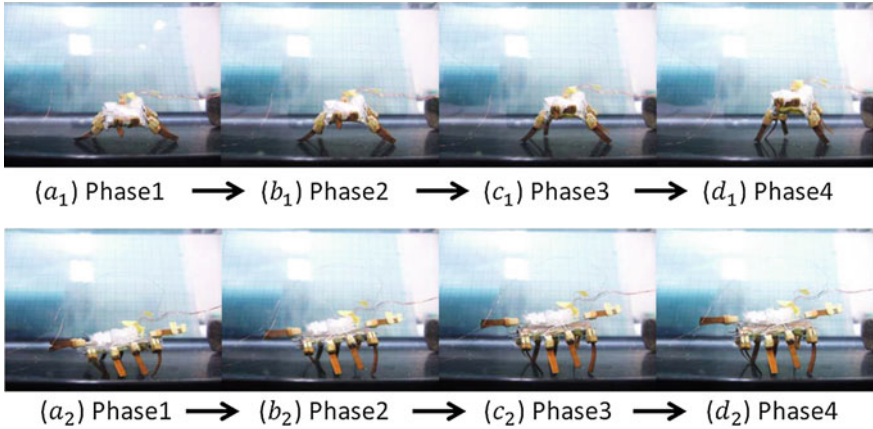


Fig. 26 Standing experiments on the underwater flat

5.5 Obstacle-Avoidance Experiment

To implement closed-loop control, we installed one short-range proximity sensor on the microrobot to detect an object or avoid an obstacle while walking or swimming. The proximity sensor used in the present research was 8 mm long and 5 mm wide, with a weight of 0.5 g. The distance measurement range was 0–60 mm, and the output voltage ranged from 150 mV to the power voltage [29]. The sensor signals were transmitted to a micro-AD board, which converted the voltages to digital values and sent them to the AVR. By utilizing the proximity sensor, the microrobot was able to detect an obstacle in front of it without any physical contact, and avoided it automatically. In the previous experiments, the microrobot avoided an obstacle by changing its walking direction. However, due to the low rotating efficiency of this unit while in a standing attitude, a long time was required to avoid a very wide obstacle via rotation. Therefore, the hybrid robot avoided the obstacle by floating instead. Figure 27 shows the object-avoidance experiment in the standing attitude. First, the microrobot walked toward the obstacle using legs A, D, E, and H driven by an input voltage of 6 V at a frequency of 1 Hz. When the distance between the microrobot and the obstacle decreased to about 10 mm, the proximity sensor detected the obstacle. The microrobot then stopped and floated upward.

5.6 Swimming Experiments in the Standing Attitude

The swimming experiments were carried out in the same water tank. To increase the oscillatory thrust, the swimming motion was evaluated in the standing attitude.

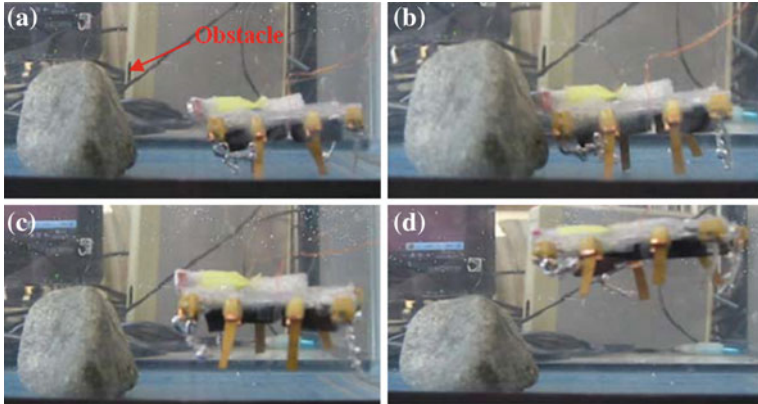


Fig. 27 *Obstacle avoidance experiment. a* Walking forward. *b* Detected the obstacle. *c* Floating upward. *d* Floating state

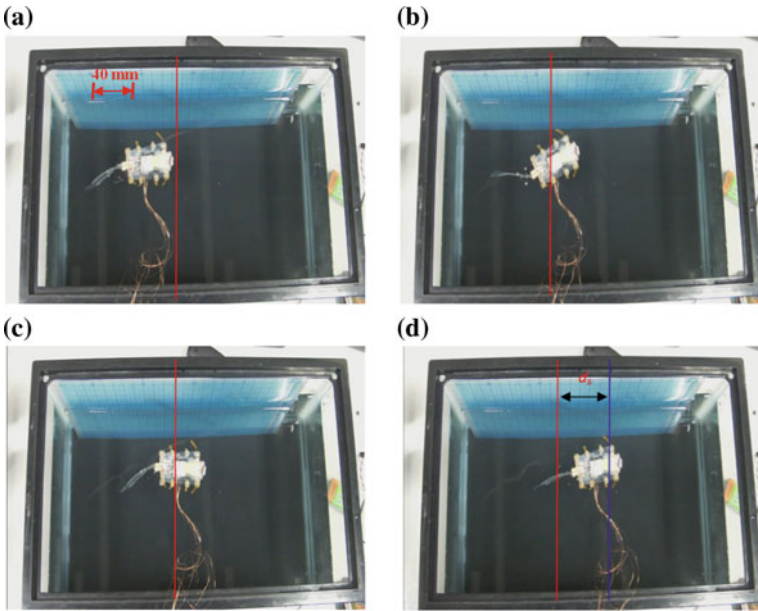


Fig. 28 *Swimming experiment. a* Initial position (*red line*). *b* *Left bending*. *c* *Right bending*. *d* Final position (*blue line*)

Water resistance increases in proportion to the cross-sectional area of the robot body, reducing the oscillatory amplitude of the body. On the other hand, increasing the oscillatory amplitude can reduce the effect of water resistance and increase the swimming speed. The IPMC actuator was actuated by a square-wave signal with a frequency of 0.5 Hz and an input voltage of 6 V. The swimming motion for one oscillatory cycle is shown in Fig. 28.

6 Results and Discussion

Generally speaking, compact structure, multifunctionality, flexibility, and precise positioning are considered incompatible characteristics in underwater microrobots [39, 40]. We have already designed several bio-inspired underwater robots with compact structures using IPMC and SMA actuators. These robots employ biomimetic locomotion to implement walking/rotating, surfacing/diving, grasping, and swimming motions. However, each of the units implements only some of these motions. To design a robot with multifunctionality, we need to integrate the above motions in a single robot. There are three types of underwater walking/rotating motions: inchworm-inspired, stick-insect-inspired, and lobster-inspired. Since the position precision of IPMC legs has not been high, in the present research we proposed an electromechanical model of an IPMC leg for position control [29]. Also, a novel hybrid structure with two motion attitudes was developed to adapt to different environments. Floating can be achieved via the electrolysis characteristics of IPMC, or via jellyfish-inspired or fish-bladder-inspired designs. Since the floating speeds are adjustable in all three of these methods, the first is the best choice to realize a compact structure. Swimming can be achieved via fish-inspired, snake-inspired, butterfly-inspired, or manta-ray-inspired designs. However, due to mechanism limitations, only a caudal actuator was suitable for our hybrid design. Accordingly, we used a single IPMC actuator to drive a passive fin in an oscillatory motion. Human-inspired, inchworm-inspired, and lobster-inspired finger locomotion have been proposed for grasping. Our new design not only inherited lobster-inspired finger locomotion, but also implemented inchworm-inspired grasping motion by changing its attitude from lying to standing. Also, a schematic diagram of the Father–son robot system is shown in Fig. 29.

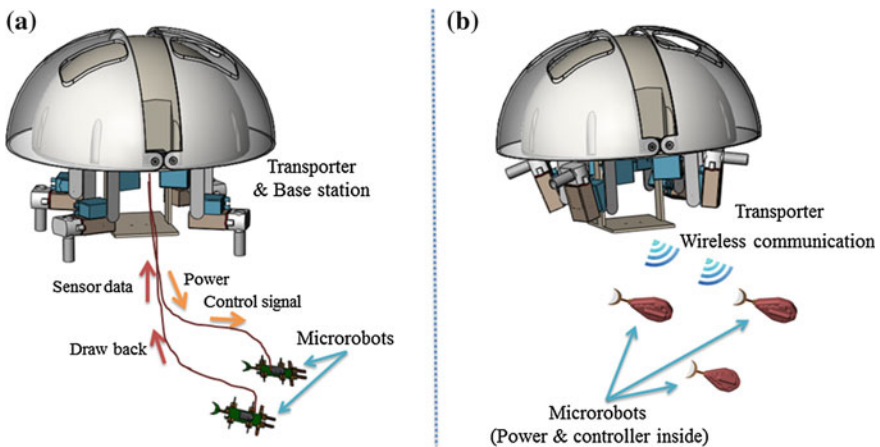


Fig. 29 A schematic diagram of the father–son robot system. **a** Wire communication. **b** Wireless communication

7 Conclusion

In this chapter, stick insect-inspired two-phase walking locomotion, jellyfish-inspired floating/diving locomotion, and inchworm-inspired crawling and grasping locomotion were discussed. The feasibility results for four previously developed prototype microrobots were then reviewed. The floating efficiency of a stick insect-inspired robot was not high. A jellyfish-like robot could not rotate and its walking motion was unsatisfactory, although its floating motion was improved. For an inchworm-inspired robot, there were large differences in the rotational radii of the outside four legs, leading to a large amount of slippage while rotating and low rotating efficiency. In addition, the inside six legs were used solely as fingers to grasp an object and could not contribute any buoyancy to the floating motion, so that the floating speed was slow. To inherit the multifunctions of the inchworm-inspired microrobot and overcome its disadvantages, we introduced a new lobster-like microrobot, intended for underwater exploration in a restricted space.

Then, we introduced a hybrid biomimetic microrobot with two motion attitudes to implement microrobot multifunctionality and flexibility for adaptation to complex underwater environments. In the lying attitude, the new robot implemented stick-insect-inspired walking/rotating motions using eight IPMC legs. These legs were also used to electrolyze the water for floating. Two lobster-inspired IPMC fingers were used to grasp small objects. According to the results of the walking experiments, the robot reached a maximum walking speed of 3.6 mm/s at a control frequency of 2.5 Hz and a fixed current of 0.7 A. The results of the floating experiments indicated that the robot could achieve a maximum floating speed at a control frequency of 0.05 Hz and a control voltage of 6 V. Driven by two SMA actuators, the robot could change its attitude from lying to standing on an underwater flat. In the standing attitude, the microrobot could implement inchworm-inspired walking/rotating using the four outside IPMC legs. The four inside legs were utilized as fingers to grasp large objects. While suspended in the water, the IPMC caudal fin actuated a passive fin to implement oscillatory motion, which provided propulsion for swimming. When equipped with a proximity sensor, the robot could detect and avoid obstacles automatically, either by rotating or by floating.

As the next step in our research, we will introduce the father–son robot system to solve microrobot design problems requiring as low speeds and short operating times in restricted operating areas.

Acknowledgments This research is partly supported by National Natural Science Foundation of China (61375094), Key Research Program of the Natural Science Foundation of Tianjin (13JCZDJC26200) and National High Tech. Research and Development Program of China (No.2015AA043202).

References

1. Shi L, Guo S, Asaka K (2011) Development of a new jellyfish-type underwater microrobot. *Int J Robot Autom* 26(2):229–241
2. Guo S, Shi L, Asaka K, Li L (2009) Experiments and characteristics analysis of a bio-inspired underwater microrobot. In: Proceedings of the 2009 IEEE international conference on mechatronics and automation, Changchun, China, 9–12 August 2009
3. Lin X, Guo S (2012) Development of a spherical underwater robot equipped with multiple vectored water-jet-based thrusters. *J Intell Rob Syst* 67(3–4):307–321
4. Shi L, Guo S, Mao S, Li M, Asaka K (2013) Development of a lobster-inspired underwater microrobot. *Int J Adv Rob Syst* 10:1–15. doi:10.5772/54868
5. Cavallo E, Michelini R, Filaretov V (2004) Conceptual design of an AUV equipped with a three degrees of freedom vectored thrusters. *J Intell Robot Syst* 39(4):365–391
6. Duchemin O, Lorand A, Notarianni M, Valentian D, Chesta E (2007) Multi-channel hall-effect thrusters: mission applications and architecture trade-offs. In: Proceedings of the 30th international electric propulsion conference, Florence, Italy, 17–20 September 2007
7. Behkam B, Sitti M (2006) Design methodology for biomimetic propulsion of miniature swimming robots. *J Dyn Syst Meas Contr* 128(1):36–43
8. Zhang W, Guo S, Asaka K (2006) A new type of hybrid fish-like microrobot. *Int J Autom Comput* 3(4):358–365
9. Heo S, Wiguna T, Park H, Goo N (2007) Effect of an artificial caudal fin on the performance of a biomimetic fish robot propelled by piezoelectric actuators. *J Bionic Eng* 4(3):151–158
10. Villanueva A, Joshi K, Blottman J, Priya S (2010) A bio-inspired shape memory alloy composite (BISMALC) actuator. *Smart Mater Struct* 19(025013):1–17
11. Wang Z, Hang G, Li J, Wang Y, Xiao K (2008) A micro-robot fish with embedded SMA wire actuated flexible biomimetic fin. *J Sens Actuators A Phys* 144(2):354–360
12. Lee S, Kim K, Park I (2007) Modeling and experiment of a muscle-like linear actuator using an ionic polymer–metal composite and its actuation characteristics. *J Smart Mater Struct* 16(3):583–588
13. Liu S, Lin M, Zhang Q (2008) Extensional ionomeric polymer conductor composite actuators with ionic liquids. *Electroact Polym Actuators Devices (EAPAD) 6927:69270H*
14. Nakadoi H, Sera A, Yamakita M, Asaka K, Luo Z, Ito K (2007) Integrated actuator-sensor system on patterned IPMC film: consideration of electronic interference. In: Proceedings of the 2007 4th IEEE international conference on mechatronics, 8–10 May 2006
15. McGovern ST, Spinks GM, Xi B, Alici G, Truong V, Wallace GG (2008) Fast bender actuators for fish-like aquatic robots. *Electroact Polym Actuators Devices (EAPAD) 6927:69271L*
16. Kamamichi N, Yamakita M, Asaka K, Luo Z (2006) A snake-like swimming robot using IPMC actuator/sensor. In: Proceedings of the 2006 IEEE international conference on robotics and automation, Orlando, Florida, USA, 15–19 May 2006
17. Kim B, Kim D, Jung J, Park J (2005) A biomimetic undulatory tadpole robot using ionic polymer–metal composite actuators. *J Smart Mater Struct* 14:1579–1585
18. Ye X, Su Y, Guo S, Wang L (2008) Design and realization of a remote control centimeter-scale robotic fish. In: Proceedings of the 2008 IEEE/ASME international conference on advanced intelligent mechatronics, Xi'an, China, 2–5 July 2008
19. Yim W, Lee J, Kim KJ (2007) An artificial muscle actuator for biomimetic underwater propulsors. *J Bioinspiration Biomimetics* 2(2):S31–S41
20. Ye X, Hu Y, Guo S, Su Y (2008) Driving mechanism of a new jellyfish-like microrobot. In: Proceedings of 2008 IEEE International Conference on Mechatronics and Automation, Takamatsu, Japan, 5–8 Aug 2008
21. Kamamichi N, Kaneda Y, Yamakita M, Asaka K, Luo ZW (2003) Biped walking of passive dynamic walker with IPMC linear actuator. In: Proceedings of SICE Annual Conference in Fukui, Fukui University, Japan, 4–6 Aug 2003

22. Shi L, Guo S, Mao S, Yue C, Li M, Asaka K (2013) development of an amphibious turtle-inspired spherical mother robot. *J Bionic Eng* 10(4):446–455
23. Guo S, Mao S, Shi L, Li M (2012) Development of an amphibious mother spherical robot used as the carrier for underwater microrobots, In: Proceedings of the 2012 ICME International Conference on Complex Medical Engineering, Kobe, Japan, 1–4 July 2012
24. Guo S, Mao S, Shi L, Li M (2012) Design and kinematic analysis of an amphibious spherical robot. In: Proceedings of 2012 IEEE International Conference on Mechatronics and Automation, Chengdu, China, 5–8 August 2012
25. Zhang W, Guo S, Asaka K (2006) Development of an underwater biomimetic microrobot with both compact structure and flexible locomotion. *J Microsyst Technol* 13(8):883–890
26. Shi L, Guo S, Asaka K (2010) A novel multifunctional underwater microrobot. In: Proceedings of the 2010 IEEE International Conference on Robotics and Biomimetics, Tianjin, China, 14–18 Dec 2010
27. Shi L, Guo S, Asaka K (2012) A novel jellyfish- and butterfly-inspired underwater microrobot with pectoral fins. *Int J Robot Autom* 27(3):276–286
28. Gong Y, Fan J, Tang C, Tsui C (2011) Numerical simulation of dynamic electro-mechanical response of ionic polymer-metal composites. *J Bionic Eng* 8:263–272
29. Shi L, Guo S, Li M, Mao S, Xiao N, Gao B, Song Z, Asaka K (2012) A novel soft biomimetic microrobot with two motion attitudes. *Sensors* 12(12):16732–16758
30. Shi L, Guo S, Kudo H, Asaka K (2012) Development of a venus flytrap-inspired robotic flytrap. In: Proceedings of the 2012 IEEE international conference on robotics and biomimetics, Guangzhou, China, 11–14 Dec 2012
31. Gao B, Guo S (2010) Development of an infrared ray controlled fish-like underwater microrobot. In: Proceedings of the 2010 IEEE International Conference on Automation and Logistics, Hong Kong and Macau, China, 16–20 Aug 2010
32. Gao B, Guo S, Ye X (2011) Motion-control analysis of ICPF-actuated underwater biomimetic microrobots. *Int J Mechatron Autom* 1(2):79–89
33. Shi L, Guo S, Asaka K (2011) A novel butterfly-inspired underwater microrobot with pectoral fins. In: Proceedings of the 2011 IEEE International Conference on Mechatronics and Automation, Beijing, China, 7–10 Aug 2011
34. Shi L, Guo S, Asaka K (2011) A bio-inspired underwater microrobot with compact structure and multifunctional locomotion. In: Proceedings of 2011 IEEE/ASME International Conference on Advanced Intelligent Mechatronics (AIM 2011), Budapest, Hungary, 3–7 July 2011
35. Guo S, Shi L, Xiao N, Asaka K (2012) A biomimetic underwater microrobot with multifunctional locomotion. *Robot Auton Syst* 60(12):1472–1473
36. Gao B, Guo S (2011) Dynamic mechanics and electric field analysis of an ICPF actuated fish-like underwater microrobot. In: Proceeding of the IEEE International Conference on Automation and Logistics, Chongqing, China, 15–18 Aug 2011
37. Guo S, Li M, Shi L, Mao S (2012) A smart actuator-based underwater microrobot with two motion attitudes. In: Proceedings of 2012 IEEE International Conference on Mechatronics and Automation, Chengdu, China, 5–8 Aug 2012
38. Chu W, Lee K, Song S, Han M, Lee J, Kim H, Kim M, Park Y, Cho K, Ahn S (2012) Review of biomimetic underwater robots using smart actuators. *Int J Precis Eng Manuf* 13(7):1281–1292
39. Shi L, Guo S, Asaka K (2012) Modeling and experiments of IPMC actuators for the position precision of underwater legged microrobots. In: Proceedings of the 2012 IEEE International Conference on Automation and Logistics, Zhengzhou, China, 15–17 Aug 2012
40. Park I, Kim S, Kim D, Kin K (2007) The mechanical properties of ionic polymer-metal composites. *J Electroact Polym Actuators Devices (EAPAD)* 6524:65241R